Published in final edited form as:
Clin Cancer Res. 2022 November 01; 28(21): 4820–4831. doi:10.1158/1078-0432.CCR-22-1362.

Phototherapy with cancer-specific nanoporphyrin potentiates immunotherapy in bladder cancer

Zheng Zhu[1,2,#], **Ai-Hong Ma**[3,#], **Hongyong Zhang**[3,#], **Tzu-Yin Lin**[4], **Xiangdong Xue**[3,5], **Hizra Farrukh**[1,2], **Shaoming Zhu**[6,7], **Wei Shi**[6,8], **Ruan Yuan**[6,9], **Zhixiu Cao**[6,10], **Veera Chandra Sekhar Reddy Chittepu**[1,2], **Rao Prabhala**[2,11], **Yuanpei Li**[3], **Kit S. Lam**[3], **Chong-xian Pan**[1,2,*]

[1.] Brigham and Women's Hospital, Harvard Medical School, Boston, MA 02115, USA.

[2.] VA Boston Healthcare System, 1400 VFW Parkway Building 3, Room 2B-110, West Roxbury, MA 02132, USA

[3.] Department of Biochemistry and Molecular Medicine, University of California Davis, Sacramento, CA 95817, USA

[4.] Division of Hematology and Oncology, Department of Internal Medicine, School of Medicine, University of California Davis, Sacramento, CA 95817, USA

[5.] School of Pharmacy, Pharm-X Center, Shanghai Jiao Tong University, Shanghai, 200240, China

[6.] Department of Internal Medicine, University of California Davis, Sacramento, CA 95817, USA

[7.] Department of Urology, Beijing Chao-Yang Hospital, Capital Medical University, NO.8 GongTi South Road, Beijing 100020, China.

[8.] Department of Neurosurgery, 960th hospital of PLA, Shifan road, Jinan city, Shandong province,250000, China

[9.] Department of Urology, Renmin Hospital of Wuhan University, Wuhan 430200, China

[10.] Department of Urology, Wuhan NO.1 Hospital, Wuhan,Hubei, 430022, China.

[11.] Dana-Farber Cancer Institute, Harvard Medical School, Boston, MA, USA

Abstract

Purpose: Immune checkpoint inhibitors (ICIs) in general have shown poor efficacy in bladder cancer (BCa). The purpose of this project was to determine whether photodynamic therapy (PDT) with BCa-specific porphyrin-based PLZ4-nanoparticles (PNP) potentiated ICI.

Experimental Design: SV40 T/Ras double-transgenic mice bearing spontaneous BCa and C57BL/6 mice carrying syngeneic bladder cancer models were used to determine the efficacy and conduct molecular correlative studies.

[*]Corresponding author Dr. Chong-xian Pan, Harvard Medical School, 1400 VFW Parkway Building 3, Room 2B-110, West Roxbury, MA 02132, USA. Phone: (617) 323-7700. chongxian_pan@hms.harvard.edu.
[#]Equal contribution.

Conflicts of interest
Drs. Pan, Lam and Zhang are co-inventors of the PLZ4 peptide used for this study; Drs. Lam, Li, Pan and Lin are co-inventors of nanoporphyrin; Drs. Pan, Lam, Li and Lin are co-founders of LP Therapeutics that licensed PLZ4 therapeutics. Dr. Lam is the founder of LamnoTherapeutics that licenses nanoporphyrin. The remaining authors declare no potential conflicts of interest.

Results: PDT with PNP generated reactive oxygen species, induced protein carbonylation and dendritic cell maturation. In SV40 T/Ras double-transgenic mice carrying spontaneous bladder cancer, the median survival was 33.7 days in the control, compared to 44.8 (p=0.0123), 52.6 (p=0.0054) and over 75 (p=0.0001) days in the anti-programmed cell death-1 antibody(anti-PD-1), PNP PDT and combination groups, respectively. At Day 75 when all mice in other groups died, only one in 7 mice in the combination group died. For the direct anti-tumor activity, compared to the control, the ani-PD-1, PNP PDT and combination groups induced a 40.25% (p=0.0003), 80.72% (p<0.0001) and 93.03% (p<0.0001) tumor reduction, respectively. For the abscopal anti-cancer immunity, the anti-PD-1, PNP PDT and combination groups induced tumor reduction of 45.73% (p=0.0001), 54.92% (p<0.0001) and 75.96% (p<0.0001), respectively. The combination treatment also diminished spontaneous and induced lung metastasis. Potential of immunotherapy by PNP PDT is multifactorial.

Conclusions: In addition to its potential for photodynamic diagnosis and therapy, PNP PDT can synergize immunotherapy in treating locally advanced and metastatic bladder cancer. Clinical trials are warranted to determine the efficacy and toxicity of this combination.

Keywords

photodynamic therapy; immunotherapy; nanoparticle; checkpoint inhibitor; bladder cancer

INTRODUCTION

Bladder cancer (BCa) is one of the top ten most common cancers. It is estimated that approximately 81,180 new cases will be diagnosed with 17,100 deaths from BCa in the US in 2022 [1]. Immunotherapy with immune checkpoint inhibitors (ICIs) plays major roles in the management of BCa from early-stage non-muscle-invasive bladder cancer (NMIBC), to locally advanced and metastatic BCa. However, the efficacy of ICIs is, in general, disappointing. For NMIBC unresponsive to Bacillus Calmette-Guérin (BCG) therapy, salvage anti-programmed cell death 1 (PD-1) antibody pembrolizumab intravenous treatment has a response rate of 40%, and less than 20% of patients retain response for 12 months or more [2]. For patients with advanced or metastatic BCa who do not have any disease progression after chemotherapy, anti-programmed death ligand-1 (PD-L1) antibody avelumab significantly improves the overall survival from 14 months of the best supportive care group to 21 months. Nevertheless, its median progression-free survival is only 3.7 months and objective response rate less than 10% [3]. Anti-PD-1/PD-L1 antibodies are also used in patients who have disease progression after chemotherapy (if they do not receive ICI before), or cisplatin-ineligible patients whose cancer expresses PD-L1 or chemotherapy-ineligible patients. In all these treatments, ICIs as a single agent have the response rate of only around 20% [4–10]. Hence, there is a dire unmet need for strategies to enhance the efficacy of ICIs to improve the overall treatment outcomes of BCa of all stages.

BCa is an ideal disease for photodynamic diagnosis (PDD) and therapy (PDT) as it is already accessed by light and directly visualized during cystoscopy. PDD and PDT rely on cancer-specific accumulation of a photosensitizer that, when activated by light, emits fluorescence for PDD and generates reactive oxygen species (ROS) to kill cells for PDT. PDD with blue light cystoscopy and PDT have been widely studied for bladder diseases

[11–14]. However, current photosensitizers have poor selectivity, a low absorption band, poor bioavailability, and low efficiency [15]. It has been shown that the difference of photosensitizer accumulation between cancer cells and normal cells is only 2–3 times [16], and many non-cancerous conditions, such as infection and inflammation, can increase non-specific uptake of photosensitizers. Hence, blue light cystoscopy has limited clinical applications, and PDT has not been approved for BCa in the United States.

Recently we developed a BCa-targeting peptide named PLZ4 (amino acid sequence: cQDGRMGFc, in which two small letters of "c" represent D-cysteine and capital letters represent L-amino acids) that binds to $\alpha_v\beta_3$ integrin [17, 18]. It can specifically bind to human, dog and mouse BCa cells, but not to the confounding cells, such as normal urothelial cells, blood cells, fibroblasts, human vascular endothelial cells and inflammation cells from a dog with chronic cystitis. We subsequently developed a porphyrin-based nanometer-scale micelles that are decorated with PLZ4 on the surface for cancer-specific targeting. This PLZ4-nanoporphyrin (PNP) can be used for PDD, PDT and photothermal therapy in addition to many other applications [19–22]. Compared to only a 2–3-fold difference of accumulation between cancer and non-cancer cells of photosensitizers currently used in clinics, PNP achieves cancer-specific delivery 30–40 times more to adjacent normal urothelial cells in vivo. Furthermore, its potency increases by over 100-folds. PNP has already reached the IND (Investigational New Drug)-enabling pharmacology and toxicology studies supported by a Department of Defense grant.

Several studies showed that PDT can potentiate immunotherapy [23–28]. PDT kills cancer cells, induces immunogenic cell death, releases tumor antigens, stimulates innate immunity as well as adaptive immune response (Reviewed in [29]). In this project, we aimed to determine whether PDT with PNP could potentiate ICIs in addition to its potential use of PDD and PDT in BCa. If so, PNP can be developed to enhance the efficacy of ICIs along with PDD and PDT.

MATERIALS AND METHODS

Preparation of PLZ4-nanoporphyrin (PNP)

The pyropheophorbide a (Por)-containing telodendrimer (PEG^{5k}-Por_4-CA_4) was synthesized via a solution-phase condensation reaction according to our established method [20]. PLZ4-PEG^{5k}-CA_8 telodendrimer was synthesized by conjugation of alkyne-derivatized PLZ4 (CPC scientific, Sunyvale, CA) to PEG^{5k}-CA_8 telodendrimer via click chemistry. PNP was obtained via a mixed micelle strategy. Briefly, 10 mg PLZ4-PEG^{5k}-CA_8 and 10 mg PEG^{5k}-Por_4/CA_4 were dissolved in chloroform and evaporated on a rotavapor to obtain a homogeneous dry polymer film. The film was reconstituted in 1 ml phosphate-buffered solution (PBS) with sonication to disperse into PNP solution.

PNP characterization

The morphology and structure of PNP were examined by transmission electron microscopy (TEM, Talos L120C, FEI). Dynamic light scattering (DLS) was performed to measure the hydrodynamic particle size by Zetasizer NanoZS (Malvern). The UV-vis spectra were

measured with a spectrometer (UV-1800, Shimadzu). The absorbance range was set as 800 nm to 220 nm. The fluorescence spectra were collected by a fluorescence spectrometer (RF-6000. Shimadzu). The excitation was set as 412 nm, and the emissive band was set from 432 nm to 800 nm.

Cell lines and reagents

BBN963 murine BCa cell line was kindly provided by William Kim, MD, Ph.D. at University of North Carolina[30]. MB49 murine BCa cell line (SCC148, RRID: CVCL_7076) and DC 2.4 murine dendritic cell line (SCC142, RRID: CVCL_J409) were purchased from Sigma. Once the cell lines were received, they were immediately expanded with freshly prepared medium, and 20–30 vials were cryopreserved in liquid nitrogen to ensure that each batch of cells was used within a few months. Mycoplasma test was performed with the PlasmoTest™ kit (InvivoGen. Cat log No: rep-pt1) every 2–3 months. Because cell lines were used within 6 months of culture after arrival, no cell line authentication was performed. BBN963 cells were cultured with 90% DMEM+10% fetal bovine serum (FBS) and MB49 cells were cultured with 90% RPMI+10% FBS at a 37°C incubator with 5% CO_2. Anti-PD-1 antibody was purchased from BioXcell (Cat# BE0146, Lebanon, NH. RRID: AB_10949053), and administered 200 μg/mouse, intraperitoneal (i.p.) twice a week. PNP (10 μg/mL) was administered 1 μg per 10g body weight, intravenous (i.v.) once a week.

Cellular uptake

To study the cellular uptake of PNP, MB49 cancer cells seeded in glass-bottom plates (5×10^4 cells per well) were incubated with PNP (10 μg/mL) for 4 h. Then the culture medium was discarded, and the cells were washed with PBS three times. The intracellular uptake of PNP was then observed on confocal laser scanning microscopy (CLSM), (Leica, Buffalo Grove, IL).

In vitro reactive oxygen species (ROS) production

Four groups (i.e., control, control + Laser, PNP, PNP + Laser) were used to study ROS production by PNP after laser treatment. BBN963 cells were incubated with PNP (10 μg/mL) for 4h. Then the culture medium was discarded and washed by PBS. Subsequently, the culture medium was replaced by containing DCFH-DA 10 mM in 20,7'-dichlorofluorescein (DCF) (Sigma, D6883) and laser treatment 4.2 J/cm2 (Omnilux New-U LED panel with 635 nm light, Clifton Park, NY) was applied. After incubation for another 30 min, cells were washed with PBS three times and scanned by CLSM. ROS carbonylation of proteins was determined with Abcam carbonyl kit (Abcam, ab126287) per manufacturer's protocol.

In vitro dendritic cell stimulation with transwell culture

DC 2.4 cells were seeded at the lower compartment and cultured overnight. 3×10^3 BBN963 cells received one of the following four treatments: phosphate-buffered solution (PBS) control, PBS control + Laser, PNP, PNP + Laser, 24 hours prior to culture of DC 2.4 cells at the upper wells. After coculture for 24h, DC 2.4 cells were harvested and stained with

anti-CD80 PerCP/Cyanine5.5 and anti-CD86 PE/Dazzle™ 594 followed by flow cytometry (BD Fortessa) analysis.

PNP induced PDT for immune system activation

All *in vivo* experiments were performed following a protocol approved by University of California Davis IACUC (No. 17763). Eight weeks female C57BL/6 albino mice (C57BL/6BrdCrHsd-Tyr^c) were purchased from Envigo. MB49 cells (1×10^5) were injected into the right flank of the mice subcutaneously as a primary tumor. Seven days later, mice were randomized into four groups: control, anti-PD-1 (BioXcell, 200 μg i.p., twice per week), PNP (100 mg/kg in 50 μl, i.v., weekly) + Laser (L, 0.2w, 3 min) and anti-PD-1+PNP+L. Laser treatment was applied to PNP and combination groups at 24 hours post-injection of PNP. One week after the initial treatment, 1×10^5 MB49 cells were injected into the left flank as a secondary site. In total, two rounds of treatments were applied to these mice. Tumors were harvested for analysis.

Biodistribution of PNP

C57BL/6 mice carrying BBN963 syngeneic tumors were used for this study. PNP 100 mg/kg was i.v. administrated. The near-infrared fluorescence (NIRF) in tumor was monitored by animal imaging system at different time points. Mice were euthanized at 24, 48, 72 and 96 hours after PNP administration. Tumors and major organs were harvested for NIRF imaging.

PNP plus anti-PD-1 treatment for suppression of metastasis

For the lung metastasis model induced by tail vein injection, MB49 cells (1×10^6) were injected into the right flank of C57BL/6 mice. When tumor sizes reached around 100 mm^3, C57BL/6 mice were randomly divided into four groups (n=4): control, anti-PD-1, PNP+L, anti-PD-1+PNP+L. PNP was i.v. injected into the mice on days 1 and 8, followed by laser treatment 24 hours after. Anti-PD-1 treatment was applied twice a week, i.p.. After the first round of treatment, MB49 cells (1×10^6 per mouse) were injected to the left flank to determine abscopal effects. Left-side tumors were harvested on day 15 for analysis.

Similarly, MB49 cells (1×10^6) were injected into the right flank of C57BL/6 mice. When tumor sizes reached around 100 mm^3, C57BL/6 mice were randomly divided into four groups (n=5): control, anti-PD-1, PNP+L, anti-PD-1+PNP+L. PNP was i.v. injected into the mice on days 1, 8 and 15 followed by laser treatment 24 hours after. Anti-PD-1 treatment was applied twice a week, i.p.. After the first round of treatment, MB49 cells (1×10^6 per mouse) were injected via mouse tail vein on day 7 to mimic lung metastasis. Lungs were harvested on day 22 for H&E staining.

For the spontaneous lung metastasis model, MB49 cells (5×10^6) were injected into the right flank of C57BL/6 mice. When tumors reached about 100 mm^3, mice were randomly divided into four groups (n=5): control, anti-PD-1, PNP+L, anti-PD-1+PNP+L. PNP was i.v. injected into the mice on days 1, 8, and 15 followed by laser treatment 24 hours after. Anti-PD-1 treatment was applied twice a week, i.p. Lungs were harvested on day 22 for H&E staining.

PNP plus anti-PD-1 treatment for suppression of distant tumors

BBN963 cells (5×10^6) were subcutaneously injected into the right and left flanks of each C57BL/6 mice. Fourteen days later, these mice were separated into four groups (n=8 in each group): control, anti-PD-1, PNP+L, anti-PD-1+PNP+L. PNP was i.v. injected into the mice on days 1, 8, and 15. Laser treatment was applied to the tumors at the right flank 24 hours after PNP administration. Anti-PD-1 treatment was applied twice a week i.p. The tumor size was recorded as length and width, while the tumor volume was calculated as (length × width^2)/2. The effects on tumor growth at the right flank were considered direct anti-tumor activity while the effects on the left flank tumors (not treated with laser) were considered as abscopal effects).

Efficacy study in SV40T/Ras double transgenic spontaneous BCa model

Mice carrying heterozygous UPII-Ras* [Ras with codon 61 (Q > L), abbreviated as Ras*], and heterozygous UPII-SV40T transgene were obtained from Xue-Ru Wu, MD, at New York University. Mice at 7- to 8-week-old were crossbred to produce double transgenic mice. These mice were genotyped before day 21 with the primers (sequence 5'–3'): RAS-F: TCCCACTCCGAGACAAAATC; RAS-R: ATTCGTCCACGAAGTGGTTC; SV40T-F: GGAAAGTCCTTGGGGTCTTC; SV40T-R: CACTTGTGTGGGTTGATTGC. Due to technical difficulty of inserting an optical fiber into the bladder of male mice for PDT, only female double transgenic mice were used and randomized into four groups: control, anti-PD-1, PNP+L, anti-PD-1+PNP+L. PNP was intravenously injected into the mice on days 1, 8, and 15. Laser treatment followed after 24 hours. Anti-PD-1 treatment was applied on days 2, 9 and 16. Tumors were monitored by magnetic resonance imaging (MRI).

Mechanism investigation of the in vivo combined therapeutics

BBN963 cells (5×10^6) or MB49 cells (1×10^6) were subcutaneously injected into the right and left flank of each C57BL/6 mice. Right side is designed as primary tumor and treated with light and PNP or anti-PD-1 plus PNP groups while the left side is designed as secondary site with no light treatment.

Mice were treated with PBS, anti-PD-1, PNP+L, anti-PD-1+PNP+L for two weeks. Left tumors were collected to make single cell suspension. The harvested cells were analyzed by flow cytometry or cytometry by time of flight (CyTOF) and/or immunofluorescence staining. Antibodies for the tumor tissue are Zombie Aqua (Biolegend, 423102, 1:400), APC-CD3 (Biolegend, 100312, 1:100), Brilliant Violet 711-CD4 (Biolegend, 100550, 1:100), PE/Cy7-CD8a (Biolegend, 100722, 1:100), BUV395-CD45(BD, 564279, 1:100). CyTOF analysis was performed at the Human Immune Monitoring Center at Stanford University. Tumor samples were stained with antibody-polymer conjugate cocktail (Maxpar® Mouse Sp/LN Phenotyping Panel Kit, 16 Marker, #201306 Fluidigm Corporation; each at 1 μL/test) following the manual procedure. ELISA kits (R&D Systems, Mouse Luminex Discovery Assay, LXSAMSM) were used to test cytokine levels.

Immunohistochemical (IHC) staining was performed according to the manufacturer's instruction (BioGenex). IHC primary antibodies against CD8a (CST, 98941S, 1:100), Ki-67 (Abcam, ab279653, 1:1000).

Statistical analysis

Independent experiments were performed for each analysis described in this article. Student t-test was used to compare continuous parametric data between two groups, whereas one-way ANOVA was used to compare multiple groups. Overall survival of mice was analyzed using Kaplan-Meier survival curve and log-rank test. Statistical analysis was performed by GraphPad Prism 9 software.

Data Availability

The data generated in this study are available within the article and its supplementary data files.

RESULTS

Formulation and characterization of PNP

There are two dendritic oligomers or telodendrimers in PNP which self-assemble to form nanometer-scale micelles. Both telodendrimers have a linear polyethylene glycol (PEG; MW: 5,000 Dalton, PEG^{5k}). One telodendrimer has PEG conjugated with 8 cholic acid (CA) units at one end and PLZ4 at the other end ($PLZ4\text{-}PEG^{5k}\text{-}CA_8$); the other one with four CA units and four porphyrin analog pyropheophorbide-a (Ppa) units at the same end ($PEG^{5k}\text{-}CA_4/Ppa_4$). These two telodendrimers were mixed at a 1:1 ratio in an aqueous solution which self-assemble into PNP (Fig. S1a). PNP was well dispersed in the aqueous solution and showed spherical-like vesicles of about 20 nm in diameter (Fig. S1b). Dynamic light scattering demonstrated PNP is around 18 nm in diameter (Fig. S1c).

The UV absorbance of PNP showed a slightly red-shift of the Q-band of the porphyrin, as shown in Fig. S1d. The fluorescence of porphyrin in PNP was almost completely quenched due to the aggregation-induced quenching phenomenon [31]. In comparison, dissolving of PNP in ionic detergent sodium dodecyl sulfate (SDS) or organic solvent methanol (MeOH) restored strong fluorescence around 680 nm, suggesting the successful self-assembly of the nanostructures (Fig. S1e).

Internalization and biofunction of PNP

During PDT, laser activates porphyrin to produce reactive oxygen species (ROS) which can modify macromolecules and induce immunogenic cell death to trigger an immune response. To verify ROS production induced by PNP, we firstly assessed the cell uptake of PNP in murine BCa cell line BBN963. After incubating BBN963 with PNP for 6 hours, most of the PNP was internalized into cells (Fig. 1a). ROS production was subsequently detected by a ROS detecting dye 2'–7'-dichlorofluorescein diacetate (DCFH-DA)[32] in BBN963 in the presence or absence of PNP and laser. As shown in Fig. 1b, almost no ROS was detected in the control group. Very little ROS was observed in the presence of PNP without light treatment. BBN963 cells treated with Tert-Butyl Hydrogen Peroxide (TBHP) as positive control were shown in Fig. S2. In the PNP with laser treatment (PDT) group, ROS production was much higher than that in the other three groups, and at a comparable level as TBHP. To determine the modification of proteins by ROS, a protein carbonylation assay was performed and showed that more carbonylation was found in the PNP plus laser

treatment group while there was no difference between the PNP, laser treatment group and the control group (Fig. 1c). These results suggested that PNP could accumulate in cancer cells and be evoked to produce ROS which then modified proteins during PDT.

Dendritic cells (DCs) play important roles in initiating and regulating adaptive immune responses [33]. During DC maturation/activation, costimulatory molecules, such as CD80 and CD86, are upregulated [34]. To determine whether PDT could stimulate and induce DC maturation, we performed a transwell chamber experiment. Mouse BCa cell line BBN963 cells with different treatments were cultured in the upper chamber while mouse DC cell line DC 2.4 cells were incubated in the lower chamber (Fig. 1d). Flow cytometry was performed to determine CD80 and CD86 expression on DC 2.4 cells. Detailed gating information is shown in Figure S3. PDT with PNP plus light induced much more CD11c+/CD80+/CD86+ DC cells than the other three groups (Fig. 1e): 61.5%±2.04% in the PNP plus light versus 35.63%±1.89%, 36.23%±0.48% and 51.27%±0.89% in the control, control plus light and PNP groups, respectively. Representative flow cytometry results in each group were shown in Fig. S4. Compared to the control and light treatment groups, more DC maturation was observed when DCs were incubated with PNP alone (Fig S4). It is possible that natural light and microscopy examination activated PNP to produce ROS and stimulated DCs.

We hypothesized that PDT induced immunogenic cell death and released damage-associated molecular pattern (DAMP) molecules to stimulate DCs. To test this hypothesis, we determined two DAMP molecules in the lower chamber, adenosine triphosphat (ATP) and high-mobility group box 1 protein (HMGB1). Both molecules increased in the PNP+L treatment group (Fig. S5).

Synergistic antitumor activity of PDT and immunotherapy in treating spontaneous localized BCa

Next, we determined whether PDT could potentiate immunotherapy in treating spontaneous localized BCa. If complete remission can be induced with this combination, some patients may be spared from radical cystectomy, a procedure associated with the worse health-related quality of life among all cancers. The UPII-Ras* and the UPII-SV40T double transgenic mice were employed for this study as these mice consistently develop spontaneous localized BCa within one month and die from urinary obstruction within 5 weeks. Detection of restriction fragments representing the UPII-Ras* transgene (1.7 kb), the UPII-SV40T transgene (2.7 kb), and the endogenous UPII gene (1.4 kb) (Fig. S6) at the tail was used to confirm that a mouse carries both activated Ras (Ras*) and SV40T genes. First, we determined in vivo PNP delivery and distribution. After the formation of BCa was confirmed, PNP was administrated through tail vein injection (Fig. 2a). Twenty-four hours later, the bladder and major organs were harvested to determine drug delivery. Compared to a small bladder from a wild-type mouse, two bladders from double transgenic mice showed significant enlargement secondary to tumor development inside of the bladder. PNP accumulated in the neoplastic bladder after 24h (Fig. 2b). No significant PNP signal was detected in other major organs, including heart, liver, kidney, lung, testis, and intestine except cecum (Fig. S7).

At Day 23 of age, PNP was administrated through intravenous injection followed by light treatment through an optic fiber inserted into the bladder cavity 24 hours later. Anti-PD-1 antibody was applied twice a week. These treatments were repeated weekly for up to three rounds (if mice were still alive). MRI was performed to evaluate spontaneous tumor growth (Fig. 2d). Even though immunotherapy with an anti-PD-1 antibody and PDT with PNP slightly improved the overall survival (Fig. 2c), there was no significant decrease in BCa mass (Fig. 2d). In contrast, in the immunotherapy plus PDT combination group, tumor shrinkage was observed. In one mouse of the combination group that we performed serial MRI to monitor cancer progression, clearance and shrinkage to BCa was observed; the bladder cavity effective volume increased which was filled with urine in the MRI T2 imaging; and that mouse died on Day 158 (Fig. 2d). Compared to the median overall survival of 33.7 days of the control, anti-PD-1 immunotherapy and PDT improved the overall survival by 11 days and 19 days to 44.8 (p=0.0123) and 52.6 days (p=0.0054), respectively. In contrast, the combination of anti-PD-1 immunotherapy and PDT increased the overall survival by over 40 days (p=0.0001) and only one out of 7 mice died when all mice in the other three groups died and the study ended at Day 75 (Fig. 2c). These results suggest that the PDT and anti-PD-1 immunotherapy synergistically enhanced the anti-tumor effect and improved the overall survival in vivo in the spontaneous BCa model.

Synergistic direct and abscopal anti-tumor activity of PDT and immunotherapy

To accurately measure the anti-tumor activity and determine the abscopal effects, we established bilateral subcutaneous mouse BCa models using the carcinogen-induced BBN963 cells implanted at the flanks (Fig. 3a). When tumor implants were around 100 mm^3 bilaterally, mice received phosphate buffered saline (PBS), anti-PD-1, PNP or combination through intravenous injection, followed by light treatment of the tumor located on the right flank. Tumor sizes at the right flank (treated tumor) and left flank (abscopal effects) were both measured and monitored. After intravenous injection, PNP started accumulating at the tumor sites 4 hours after administration and peaked at 24 h. Starting at 8 hours, no significant PNP accumulation at other sites of the bodies was detected except at the tumors (Fig. 3b).

First, we investigated the direct anti-tumor activity of the tumors on the right flank which received light treatment. Anti-PD-1 treatment alone showed moderate anti-tumor activity. The PNP with PDT treatment significantly delayed tumor growth at the right flank (direct anti-cancer effects) while the PDT with PNP plus anti-PD-1 combination treatment further reduced tumor growth. In 4 out of 8 mice of the combination group, no tumor was palpable at the time of study termination and the remaining mice had tumors no bigger than at the study initiation while most of the control mice reached the study endpoint at Day 32 (Fig 3c and Fig S8). At 25 days, mean tumor volume on the right (treated) side were 702.06±135.54 mm^3 in control group, 419.51±94.06 mm^3 in anti-PD-1 group, 135.34±43.55 mm^3 in PNP plus light group, and 48.91±17.86 mm^3 in combination treatment group. Compared to the control, the right-site-tumors (treated, direct anti-tumor effect) of the anti-PD-1, PNP and combination groups had a 40.25% (p=0.0003), 80.72% (p<0.0001) and 93.03% (p<0.0001) reduction, respectively (Figure 3c).

Next, we determined the abscopal anti-tumor activity by monitoring tumor growth of tumors on the left flank that did not receive any laser treatment (Fig. 3d and Fig S8). At 25 days, tumor volume on the left side (untreated, abscopal effects) were 672.02±78.38 mm^3 in control group, 364.68±96.01 mm^3 in anti-PD-1 group, 302.93±92.36 mm^3 in PDT, and 161.58±67.97 mm^3 in combination treatment group. Compared to the control, the tumor reduction of the left-site-tumors (measuring the abscopal effect) in the anti-PD-1, PDT and combination groups was 45.73% (p=0.0003), 54.92% (p<0.0001) and 75.96% (p<0.0001), respectively. The tumor reduction between the PDT with PNP and anti-PD-1 therapy groups was not statistically different (p=0.8402).

To further determine whether PDT and immunotherapy could induce abscopal anti-cancer immunity, we assessed whether treatment of local MB49 tumors could prevent the formation of distant tumors after injecting cancer cells to the left flank (Fig. 4a). For this experiment, we applied two rounds of treatment (PNP injection on Day 1 and Day 8 followed by PDT 24 hours later. Anti-PD-1 treatment was applied twice a week) for the primary tumor site at the right flank. One week later (Day 7), MB49 cells were injected into the left flank to mimic distant metastasis. On day 15, left tumors were harvested and analyzed. The gross image for tumors was shown in Fig. S9. For the right (treated) site, tumor weight was 1.83±0.12 g in the control group, 0.72±0.13 g in the anti-PD-1 group, 0.78±0.14 g in the PNP+ PDT group, and 0.21±0.13 g in the combination treatment group (Figure 4b left). The combination group had smaller tumors than any other groups. For the left (distant, abscopal) site, tumor weight was 0.2±0.02 g in the control group, 0.07±0.04 g in the anti-PD-1 group, 0.05±0.01 g in the PNP+PDT group, and 0.02±0.001 g in the combination treatment group (Fig. 4b right). All three treatment groups had smaller tumors than the control ($p<0.05$), but were not statistically different among themselves. Single therapy treatment, anti-PD-1 or PDT with PNP, considerably decreased tumor growth in both primary and secondary tumors. Tumors of the combination group were significantly smaller than the control ($p<0.0001$ for the right-treated tumors and $p=0.0013$ for the left-untreated abscopal tumors). In the combination treatment group, one mouse showed a rejection at the distant site. These results indicate the combination treatment could significantly reduce distant tumor growth.

Synergistic effect of PDT and immunotherapy in prevention of induced lung metastasis

Next, we determined whether treatment of a local MB49 tumor can prevent the development of lung metastasis from an intravenous injection of MB49 cancer cells. Since intravenous injection of diluted cancer cells required a longer time to develop lung metastasis, we applied three rounds of treatment (PNP injection on Day 1, 8, 15 followed by PDT 24 hours later. Anti-PD-1 treatment was applied twice a week) on the right flank. The representative appearance of each group was shown in Fig. 4c and the gross appearance of all lungs in each group was shown in Fig. S10. There were many large nodules in control groups; the anti-PD-1 treatment group had a considerably reduced number while the PNP+PDT group had numerous but much smaller metastatic nodules. The combination treatment group had the least lung metastatic nodules (Fig 4d). The quantification of the tumor to total lung areas are shown in Fig. 4e. The tumor/lung ratio was 7.61% in the combination group, compared to 38.69%($p=0.0383$), 28.25% ($p=0.0492$) and 37.96% ($p=0.119$) of the control, anti-PD1 and PNP plus light treatment groups, respectively.

Synergistic effect of PDT and immunotherapy in prevention of spontaneous hematogenous lung metastasis

It has been shown that subcutaneous MB49 models could develop spontaneous lung metastasis [35]. To confirm, MB49 tumor implants were first established at the right flank of C57BL/6 mice. Three weeks later, PNP was injected into the tail vein. Fluorescence from PNP concentrated at the tumor sites and lungs in a time-dependent manner (Fig 4f), suggesting that spontaneous lung metastases had developed. To determine how treatments affected spontaneous lung metastasis (Fig 4g), when MB49 tumor implants reached the size of 100 mm^3, C57BL6 mice were treated with PBS control, anti-PD-1 immunotherapy, PDT and combination weekly for three rounds as described in Fig 4g. These mice did not receive intravenous injection of MB49 cells through the tail vein. On Day 22, lungs were collected in all these mice and H&E staining was performed (Fig 4h). There were metastases in the control and anti-PD-1 treatment groups while both PDT and combination treatments almost completely prevented metastasis in the lung (Fig 4i).

The effects of photodynamic therapy on tumor immune microenvironment

To analyze the immune response induced by PNP with PDT plus anti-PD-1 treatment, we tested immune cell infiltration in different mouse models.

For BBN963 mouse model, we repeated the same treatment strategy as described in Fig. 3a for three rounds of PDT to the tumors at the right flank. Twenty-four hours after last treatment, the untreated tumors at the left flank were harvested for flow cytometry by time of flight (CyTOF). Detailed gating information for CyTOF is shown in Fig. S11a. As shown in Fig. 5a, the CD3e+TCRb+T cells in the combination treatment group was 2.81% compared to 1.06%, 1.08%, and 0.79% in the control, anti-PD-1 and PDT groups, respectively. Of the T cells in the tumors, CD3e+TCRb+ CD8+ T cells in the combination treatment group was 65.2% of CD3+ cells compared to 57.5%, 37.2%, and 64.8% in the control, anti-PD-1 and PDT groups, respectively (Fig S11b). Dendritic cells were also higher in the combination treatment group at 6.62% compared to 3.90%, 4.04% and 5.25% in the control, anti-PD-1 and PNP PDT group, respectively (Fig S12). IHC staining confirmed that in the combination treatment group, more CD8+ T cells infiltrated into the untreated tumor site Fig 5b. Statistical analysis of IHC staining was shown in Fig S13.

The increased CD8+ T cell infiltration led to tumor cell death and low proliferation in the mice that received combination treatment as determined by hematoxylin and eosin (H&E) staining, Ki-67 IHC staining and TUNEL staining (Fig S14, S15). Interleukin-6 (IL-6), IL-12p70, IL-1α/IL-1F levels in serum also markedly increased in the combination treatment group (Fig S16).

We also investigated MB49 tumors for tumor immune microenvironment changes. Two weeks after control, anti-PD-1, PDT, and combination treatment of mice carrying bilateral MB49 implants, the contralateral untreated tumors were harvested and stained with CD8. As shown in Fig. 5c, there was no significant CD8+ T cells infiltration in tumors when mice were treated with IgG control, anti-PD-1 and PDT. In contrast, the PDT with PNP plus

anti-PD-1 treatment induced the CD8+ T cell infiltration in the perivascular areas (p=0.035 when compared to the control. Fig S17).

Flow cytometry of single-cell suspension from the whole tumors showed that the percentage of CD45+ leucocytes in the PDT with PNP plus anti-PD-1 treatment group was 22.60% in the distant tumors of the left flank that were not treated with light (abscopal effects), compared to 8.63% (p=0.025), 9.80% (p=0.014) and 9.97% (p=0.006) in the control, anti-PD-1 and PNP groups, respectively. Meanwhile, the percentage of CD45+CD3+CD8+ cells in the PDT with PNP plus anti-PD-1 treatment group was 1.463% of all cells in tumor, compared to 0.408% (p=0.0008), 0.826% (p=0.0351) and 0.598% (p=0.0231) in the control group, anti-PD-1 and PNP PDT groups, respectively (Fig 5d and e).

We next determined the impact of PNP with PDT on systemic immune response. An IFN-γ ELISPOT assay showed spleen cells from the combination treatment group had much higher numbers of cells producing IFN-γ (Fig S18). Positive and negative control of spleen cells were shown in Fig S19.

DISCUSSION

In our previous study, we confirmed bladder-cancer-specific PLZ4-nanoporphyrin (PNP) could specifically deliver photosensitizer to cancer cells 30–40 times higher than to adjacent normal urothelial cells in the same bladder after intravesical instillation [20], compared to only 2–3 times with other photosensitizers commonly used in clinics during photodynamic diagnosis [16]. In addition, PNP is over 100 times more potent than 5-aminolevulic acid (5-ALA) for PDT [20]. In this series of experiments, we show that PDT with PNP can not only potentiate immunotherapy in treating locally advanced BCa, but also in treating distant tumors, inducing abscopal effects and diminishing lung metastasis. This potentiation is mainly mediated through inducing immunogenic cell death, promoting dendritic cell maturation, attracting immune cell infiltration and creating a pro-immune tumor microenvironment. Our data suggest that PNP has the potential to be developed as a multi-functional theranostic platform that combines photodynamic diagnosis, PDT and potentiation of immunotherapy in a single platform to be performed in a single procedure to address multiple unmet needs of non-muscle-invasive bladder cancer (NMIBC) to locally advanced and metastatic BCa.

For NMIBC, some of the major unmet needs are incomplete resection during TUR which occurs in over one-third of patients [36], cancer recurrence in over 70 % of patients, and cancer progression to advanced stages in one-third of these patients [37]. Upon cancer recurrence after BCG, immunotherapy with pembrolizumab is at most moderately effective with a short-term response rate of 40%, but a durable (12 months or longer) response of less than 20%. Most of the patients who failed pembrolizumab undergo radical cystectomy [2]. Our previous study already showed the great potential of PNP in identifying cancer and guiding the complete resection of TUR which can potentially decrease cancer recurrence [20]. PDT with PNP is especially suitable for diffuse cancer in situ (CIS) where TUR has a limited role, but, through intravesical instillation, CIS can be directly accessed and treated by PNP and PDT. Here we describe that PDT potentiates immunotherapy. PNP has

tremendous potential to be used from upfront diagnosis and treatment of NMIBC to salvage therapy, especially in combination with an ICI.

Some of the major issues associated with locally advanced BCa (laBC) are low efficiency of neoadjuvant chemotherapy, highly morbid cystectomy and high cancer recurrence in 30–80% of patients depending on the stage of cancer at the time of cystectomy. Since cystectomy is associated with the worst health-related quality of life, most patients would tend to avoid or delay cystectomy as much as possible. Cancer immunosurveillance achieved from immunotherapy has the potential of inducing long-term remission or even complete cure, thus providing a favorable alternative to cystectomy. Neoadjuvant immunotherapy alone has similar efficacy as neoadjuvant cytotoxic chemotherapy [38, 39]. Our studies here showed that the combination of PDT and immunotherapy is highly effective in treating laBC. The median survival for the double transgenic mice with laBC is 33.7, 44.8 and 52.8 days for the control, anti-PD-1 and photodynamic therapy, respectively, while the survival for the combination group is over 75 days. When the study was terminated on Day 75, only one out of seven mice died in the combination group while all mice in the other three treatment groups had died. Longitudinal MRI was done in one mouse to determine tumor progression (Figure 3). That mouse died at Day 158. In addition, this combination therapy can prevent both induced and spontaneous lung metastasis (Figure 4). With this promising preclinical data, it is rational to develop less toxic PDT together with immunotherapy as an option for neoadjuvant therapy for laBC.

PDT is traditionally considered a local therapy. However, when combined with immunotherapy, it can induce abscopal anti-tumor activity, treat distant tumors and decrease both spontaneous and induced lung metastasis (Figures 4). This suggests that PDT in combination with immunotherapy has the potential to be developed for metastatic BCa. Cytotoxic chemotherapy is the standard of care for newly diagnosed BCa with distant metastasis with immunotherapy used as salvage therapy or for chemotherapy ineligible patients or those with PD-L1 expression. Targeted therapy and antibody-drug conjugates are other options for advanced bladder cancer [40–44], but resistance always develops. Even though immunotherapy can induce durable response, it, as a single agent, has a disappointing response rate of around 20% [4, 5, 7, 45–47]. The response rate is even lower, at less than 10%, as maintenance therapy after chemotherapy [3]. Based on our study results, the addition of PDT with PNP to immunotherapy can potentially treat both local cancer and target distant cancers.

Our study showed the mechanisms of potentiation of immunotherapy by PDT is multifactorial. PDT produces ROS that can induce carbonylation of proteins and make them more immunogenic. The transwell study showed that it could induce dendritic cell maturation and upregulation of CD80 and CD86, two molecules that provide co-stimulation signals during T cell activation. Analyses of tumor tissues showed that PDT increased immune cell infiltration into tumors. This can have tremendous impact on managing bladder cancer as both the Cancer Genome Atlas (TCGA, 408 cases) and the European Bioinformatics Institute (EBI, 476 cases) databases show over 60% of BCas have no or little immune cell infiltration at the tumor sites (immune “cold” tumors) [48]. Furthermore, PDT treatment induces systemic immune response as demonstrated by the increased

production of pro-inflammatory systemic cytokine (Fig. S12). PDT treatment also enhances the recognition of major histocompatibility complex-I (MHC-I): antigen complexes and tumor-associated antigens by immune cells [28].

One of the major strengths of this project is that we used multiple clinically relevant animal models which consistently showed the potentiation of immunotherapy by PDT, and that the mechanistic studies supported the findings. One of the potential drawbacks is the lack of human immune system in this study. As immunotherapy research requires a competent immune system, immunocompetent mice are commonly used. We previously reported using humanized mice to study immunotherapy in which immune cells were developed from human CD34 hematopoietic stem cells and cancers from human patient-derived xenografts [49]. Due to the defective thymus and lymphoid tissue in immunocompromised mice used to generate humanized mice, the immune system in those humanized mice can be significantly different from human patients and mouse immune systems.

In summary, PDT with BCa-specific PNP can potentiate immunotherapy in treating locally advanced BCa, induce abscopal anti-tumor activity for distant cancer, and decrease cancer metastasis. These synergistic anti-tumor effects are secondary to multiple underlying mechanisms of action, such as modification of macromolecules to activate dendritic cells, increase of immune cell infiltration into tumors and alteration of tumor immune microenvironment. These findings can have a tremendous impact on the management of BCa, one of the top ten most common cancers, for which immunotherapy has disappointing efficacy. We have already held a pre-IND consultation with the US Food and Drug Administration (PIND No: 132838). Currently, the IND (Investigational New Drug)-enabling pharmacology and toxicology studies of PNP are ongoing which is supported by Department of Defense. Hence, the current study can be translated into a Phase I clinical trial in the near future to address multiple unmet needs in BCa.

Supplementary Material

Refer to Web version on PubMed Central for supplementary material.

Acknowledgments

Thanks to Mingyue Li and Lutian Yao for analyzing flow cytometry data.

Financial support

This project was supported by Merit Review (Award # 1I01 BX003840 and 1I01BX001784, PI: Pan) from the United States (U.S.) Department of Veterans Affairs Biomedical Laboratory Research and Development Program, DoD (Award #: W81XWH-19–1-0204, PI: Lam and Pan), NIH (Award #: U54CA233306, PI: Pan). The contents do not represent the views of the U.S. Department of Veterans Affairs or the United States Government.

References

1. Siegel RL, et al. , Cancer statistics, 2022. CA Cancer J Clin, 2022. 72(1): p. 7–33. [PubMed: 35020204]
2. Balar AV, et al. , Pembrolizumab monotherapy for the treatment of high-risk non-muscle-invasive bladder cancer unresponsive to BCG (KEYNOTE-057): an open-label, single-arm, multicentre, phase 2 study. Lancet Oncol, 2021. 22(7): p. 919–930. [PubMed: 34051177]

3. Powles T, et al. , Avelumab Maintenance Therapy for Advanced or Metastatic Urothelial Carcinoma. N Engl J Med, 2020. 383(13): p. 1218–1230. [PubMed: 32945632]
4. Powles T, et al. , MPDL3280A (anti-PD-L1) treatment leads to clinical activity in metastatic bladder cancer. Nature, 2014. 515(7528): p. 558–62. [PubMed: 25428503]
5. Rosenberg JE, et al. , Atezolizumab in patients with locally advanced and metastatic urothelial carcinoma who have progressed following treatment with platinum-based chemotherapy: a single-arm, multicentre, phase 2 trial. Lancet, 2016. 387(10031): p. 1909–20. [PubMed: 26952546]
6. Sharma P, et al. , Nivolumab in metastatic urothelial carcinoma after platinum therapy (CheckMate 275): a multicentre, single-arm, phase 2 trial. Lancet Oncol, 2017. 18(3): p. 312–322. [PubMed: 28131785]
7. Massard C, et al. , Safety and Efficacy of Durvalumab (MEDI4736), an Anti-Programmed Cell Death Ligand-1 Immune Checkpoint Inhibitor, in Patients With Advanced Urothelial Bladder Cancer. J Clin Oncol, 2016. 34(26): p. 3119–25. [PubMed: 27269937]
8. Apolo AB, et al. , Avelumab, an Anti-Programmed Death-Ligand 1 Antibody, In Patients With Refractory Metastatic Urothelial Carcinoma: Results From a Multicenter, Phase Ib Study. Journal of clinical oncology : official journal of the American Society of Clinical Oncology, 2017. 35(19): p. 2117–2124. [PubMed: 28375787]
9. Bellmunt J, et al. , Pembrolizumab as Second-Line Therapy for Advanced Urothelial Carcinoma. N Engl J Med, 2017. 376(11): p. 1015–1026. [PubMed: 28212060]
10. Balar AV, et al. , Atezolizumab as first-line treatment in cisplatin-ineligible patients with locally advanced and metastatic urothelial carcinoma: a single-arm, multicentre, phase 2 trial. Lancet, 2017. 389(10064): p. 67–76. [PubMed: 27939400]
11. Ray ER, et al. , Hexylaminolevulinate photodynamic diagnosis for multifocal recurrent nonmuscle invasive bladder cancer. J Endourol, 2009. 23(6): p. 983–8. [PubMed: 19441882]
12. Kausch I, et al. , Photodynamic diagnosis in non-muscle-invasive bladder cancer: a systematic review and cumulative analysis of prospective studies. Eur Urol, 2010. 57(4): p. 595–606. [PubMed: 20004052]
13. Burger M, et al. , Photodynamic diagnosis of non-muscle-invasive bladder cancer with hexaminolevulinate cystoscopy: a meta-analysis of detection and recurrence based on raw data. Eur Urol, 2013. 64(5): p. 846–54. [PubMed: 23602406]
14. Manyak MJ and Ogan K, Photodynamic therapy for refractory superficial bladder cancer: long-term clinical outcomes of single treatment using intravesical diffusion medium. J Endourol, 2003. 17(8): p. 633–9. [PubMed: 14622483]
15. Ballut S, et al. , New strategy for targeting of photosensitizers. Synthesis of glycodendrimeric phenylporphyrins, incorporation into a liposome membrane and interaction with a specific lectin. Chem Commun (Camb), 2009(2): p. 224–6. [PubMed: 19099076]
16. Seidl J, et al. , Optimization of differential photodynamic effectiveness between normal and tumor urothelial cells using 5-aminolevulinic acid-induced protoporphyrin IX as sensitizer. Int J Cancer, 2001. 92(5): p. 671–7. [PubMed: 11340570]
17. Zhang H, et al. , Identification of a bladder cancer-specific ligand using a combinatorial chemistry approach. Urol Oncol, 2012. 30(5): p. 635–45. [PubMed: 20888272]
18. Lin TY, et al. , Targeting canine bladder transitional cell carcinoma with a human bladder cancer-specific ligand. Mol Cancer, 2011. 10(1): p. 9. [PubMed: 21272294]
19. Li Y, et al. , A smart and versatile theranostic nanomedicine platform based on nanoporphyrin. Nat Commun, 2014. 5: p. 4712. [PubMed: 25158161]
20. Lin TY, et al. , Novel theranostic nanoporphyrins for photodynamic diagnosis and trimodal therapy for bladder cancer. Biomaterials, 2016. 104: p. 339–51. [PubMed: 27479049]
21. Lin TY, et al. , Multifunctional targeting micelle nanocarriers with both imaging and therapeutic potential for bladder cancer. Int J Nanomedicine, 2012. 7: p. 2793–804. [PubMed: 22745542]
22. Lin TY, et al. , Tumor-targeting multifunctional micelles for imaging and chemotherapy of advanced bladder cancer. Nanomedicine (Lond), 2013. 8(8): p. 1239–51. [PubMed: 23199207]
23. Thong PS, et al. , Photodynamic-therapy-activated immune response against distant untreated tumours in recurrent angiosarcoma. Lancet Oncol, 2007. 8(10): p. 950–2. [PubMed: 17913664]

24. Abdel-Hady ES, et al. , Immunological and viral factors associated with the response of vulval intraepithelial neoplasia to photodynamic therapy. Cancer Res, 2001. 61(1): p. 192–6. [PubMed: 11196160]
25. Evans S, et al. , Effect of photodynamic therapy on tumor necrosis factor production by murine macrophages. J Natl Cancer Inst, 1990. 82(1): p. 34–9. [PubMed: 2293654]
26. Kick G, et al. , Photodynamic therapy induces expression of interleukin 6 by activation of AP-1 but not NF-kappa B DNA binding. Cancer Res, 1995. 55(11): p. 2373–9. [PubMed: 7757989]
27. Gollnick SO, et al. , Role of cytokines in photodynamic therapy-induced local and systemic inflammation. Br J Cancer, 2003. 88(11): p. 1772–9. [PubMed: 12771994]
28. Kabingu E, et al. , Enhanced systemic immune reactivity to a Basal cell carcinoma associated antigen following photodynamic therapy. Clin Cancer Res, 2009. 15(13): p. 4460–6. [PubMed: 19549769]
29. Falk-Mahapatra R and Gollnick SO, Photodynamic Therapy and Immunity: An Update. Photochem Photobiol, 2020. 96(3): p. 550–559. [PubMed: 32128821]
30. Saito R, et al. , Molecular Subtype-Specific Immunocompetent Models of High-Grade Urothelial Carcinoma Reveal Differential Neoantigen Expression and Response to Immunotherapy. Cancer research, 2018. 78(14): p. 3954–3968. [PubMed: 29784854]
31. Micali N, et al. , Evidence of the early stage of porphyrin aggregation by enhanced Raman scattering and fluorescence spectroscopy. Phys Rev E Stat Nonlin Soft Matter Phys, 2007. 76(1 Pt 1): p. 011404. [PubMed: 17677438]
32. Afonso MB, et al. , Activation of necroptosis in human and experimental cholestasis. Cell Death Dis, 2016. 7(9): p. e2390. [PubMed: 27685634]
33. Lee YS and Radford KJ, The role of dendritic cells in cancer. Int Rev Cell Mol Biol, 2019. 348: p. 123–178. [PubMed: 31810552]
34. Bjorck P, Flores-Romo L, and Liu YJ, Human interdigitating dendritic cells directly stimulate CD40-activated naive B cells. Eur J Immunol, 1997. 27(5): p. 1266–74. [PubMed: 9174620]
35. Liu YR, et al. , Enhanced metastatic potential in the MB49 urothelial carcinoma model. Sci Rep, 2019. 9(1): p. 7425. [PubMed: 31092844]
36. Herr HW, Restaging transurethral resection of high risk superficial bladder cancer improves the initial response to bacillus Calmette-Guerin therapy. J Urol, 2005. 174(6): p. 2134–7. [PubMed: 16280743]
37. Chamie K, et al. , Recurrence of high-risk bladder cancer: a population-based analysis. Cancer, 2013. 119(17): p. 3219–27. [PubMed: 23737352]
38. Necchi A, et al. , Pembrolizumab as Neoadjuvant Therapy Before Radical Cystectomy in Patients With Muscle-Invasive Urothelial Bladder Carcinoma (PURE-01): An Open-Label, Single-Arm, Phase II Study. J Clin Oncol, 2018. 36(34): p. 3353–3360. [PubMed: 30343614]
39. Grossman HB, et al. , Neoadjuvant chemotherapy plus cystectomy compared with cystectomy alone for locally advanced bladder cancer. N Engl J Med, 2003. 349(9): p. 859–66. [PubMed: 12944571]
40. Loriot Y, et al. , Erdafitinib in Locally Advanced or Metastatic Urothelial Carcinoma. N Engl J Med, 2019. 381(4): p. 338–348. [PubMed: 31340094]
41. Powles T, et al. , Enfortumab Vedotin in Previously Treated Advanced Urothelial Carcinoma. N Engl J Med, 2021. 384(12): p. 1125–1135. [PubMed: 33577729]
42. Tagawa ST, et al. , TROPHY-U-01: A Phase II Open-Label Study of Sacituzumab Govitecan in Patients With Metastatic Urothelial Carcinoma Progressing After Platinum-Based Chemotherapy and Checkpoint Inhibitors. J Clin Oncol, 2021. 39(22): p. 2474–2485. [PubMed: 33929895]
43. Zeng SX, et al. , The Phosphatidylinositol 3-Kinase Pathway as a Potential Therapeutic Target in Bladder Cancer. Clin Cancer Res, 2017. 23(21): p. 6580–6591. [PubMed: 28808038]
44. Zhu S, et al. , Synergistic antitumor activity of pan-PI3K inhibition and immune checkpoint blockade in bladder cancer. J Immunother Cancer, 2021. 9(11).
45. Bellmunt J, et al. , Pembrolizumab as Second-Line Therapy for Advanced Urothelial Carcinoma. N Engl J Med, 2017. 376(11): p. 1015–1026. [PubMed: 28212060]

46. Sharma P, et al. , Nivolumab monotherapy in recurrent metastatic urothelial carcinoma (CheckMate 032): a multicentre, open-label, two-stage, multi-arm, phase 1/2 trial. Lancet Oncol, 2016. 17(11): p. 1590–1598. [PubMed: 27733243]

47. Balar AV, et al. , Atezolizumab as first-line treatment in cisplatin-ineligible patients with locally advanced and metastatic urothelial carcinoma: a single-arm, multicentre, phase 2 trial. Lancet, 2017. 389(10064): p. 67–76. [PubMed: 27939400]

48. Meng J, et al. , Tumor immune microenvironment-based classifications of bladder cancer for enhancing the response rate of immunotherapy. Mol Ther Oncolytics, 2021. 20: p. 410–421. [PubMed: 33665361]

49. Wang M, et al. , Humanized mice in studying efficacy and mechanisms of PD-1-targeted cancer immunotherapy. The FASEB Journal, 2018. 32(3): p. 1537–1549. [PubMed: 29146734]

Statement of Translational Relevance

Immunotherapy with immune checkpoint inhibitors (ICIs) has tremendously changed bladder cancer (BCa) management, however, with disappointing efficacy. Despite BCa being an ideal disease for photodynamic diagnosis and therapy (PDT), PDT is not yet approved mainly owing to poor tumor specificity. We developed BCa-specific porphyrin-based PLZ4-nanoparticle (PNP for PLZ4-nanoporphyrin) that, compared to existing photosensitizers used at clinic, has over 10-fold improvement in cancer specificity and 100-fold in potency. As PDT induces immunogenic cell death, makes macromolecules immunogenic with reactive oxygen species and modifies tumor microenvironment, we hypothesized that PDT with PNP potentiated immunotherapy. Using clinically relevant BCa models, we found that PDT potentiates immunotherapy in eliciting local anti-tumor immunity in both subcutaneous syngeneic and spontaneous transgenic BCa models, inducing abscopal effects, diminishing lung metastasis in both induced and spontaneous models. Accomplishment of ongoing pharmacology and toxicology studies will lead to a Phase I clinical trial in the near future.

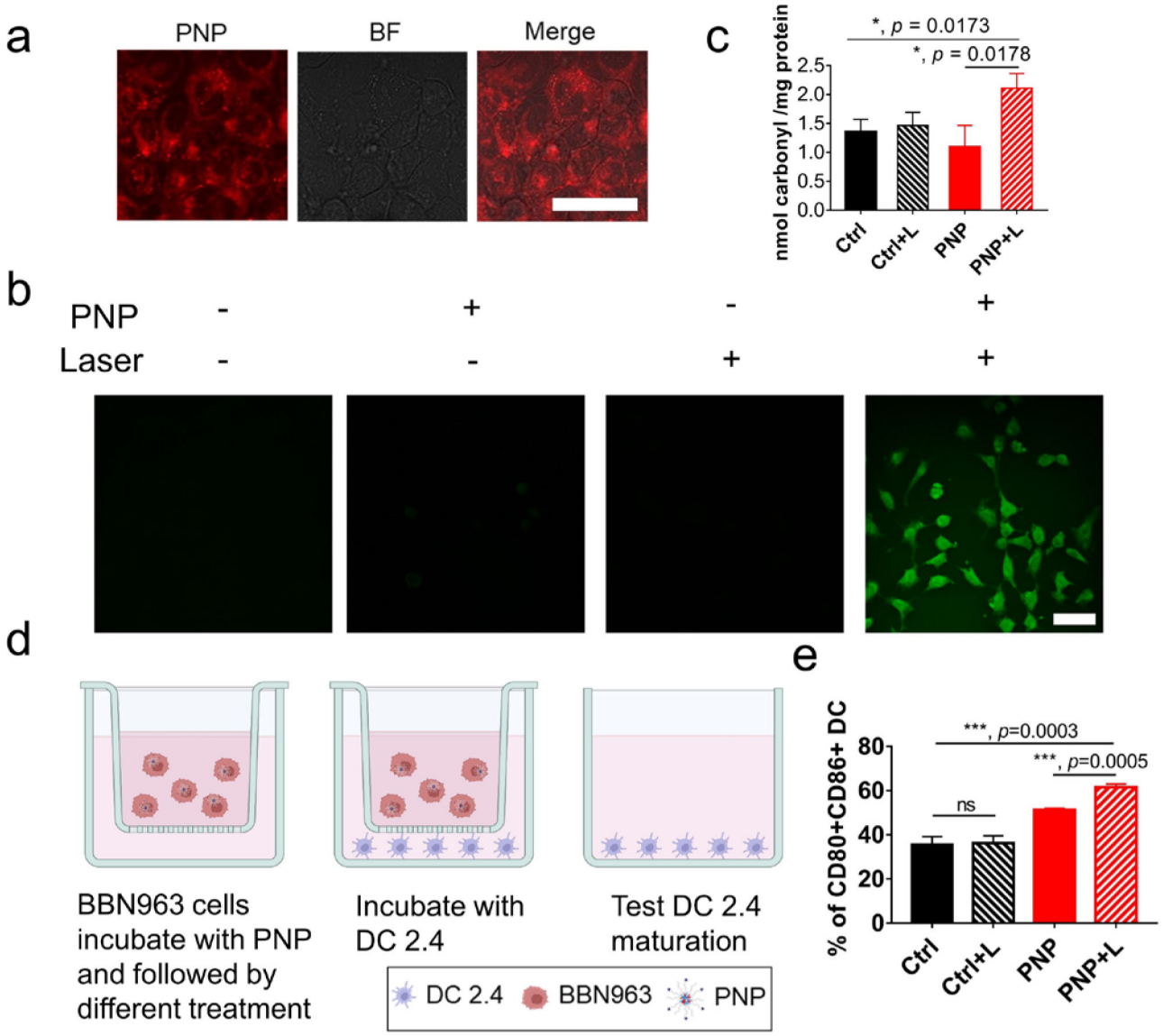

Figure 1: ROS production, protein carbonylation and stimulation of dendritic cells during PDT with PNP.

a) Confocal images of PNP uptake in BBN963 cells (scale bar=50μm), BF: bright field. **b)** ROS production after different treatments as determined by the DCFH-DA assay as determined by confocal laser scanning microscopy (scale bar=50μm). Green fluorescence indicates ROS production. Significantly more abundant ROS production was observed in the cells treated with PNP plus light. **c)** Protein carbonylation by ROS in BBN963 cells. **d)** A transwell assay to determine dendritic cell maturation. **e)** Flow cytometry analysis of CD80 and CD86 expression to determine dendritic cell maturation after different treatments for 24h in the transwell system. In the PNP + Light treatment group, 61.5%±2.04% cells expressed CD80 and CD86, compared to 35.63%±1.89%, (p=0.0003), 36.23%±0.48% (p=0.0003) and 51.27%±0.89% (p=0.0005) of the control, control plus light and PNP groups, respectively.

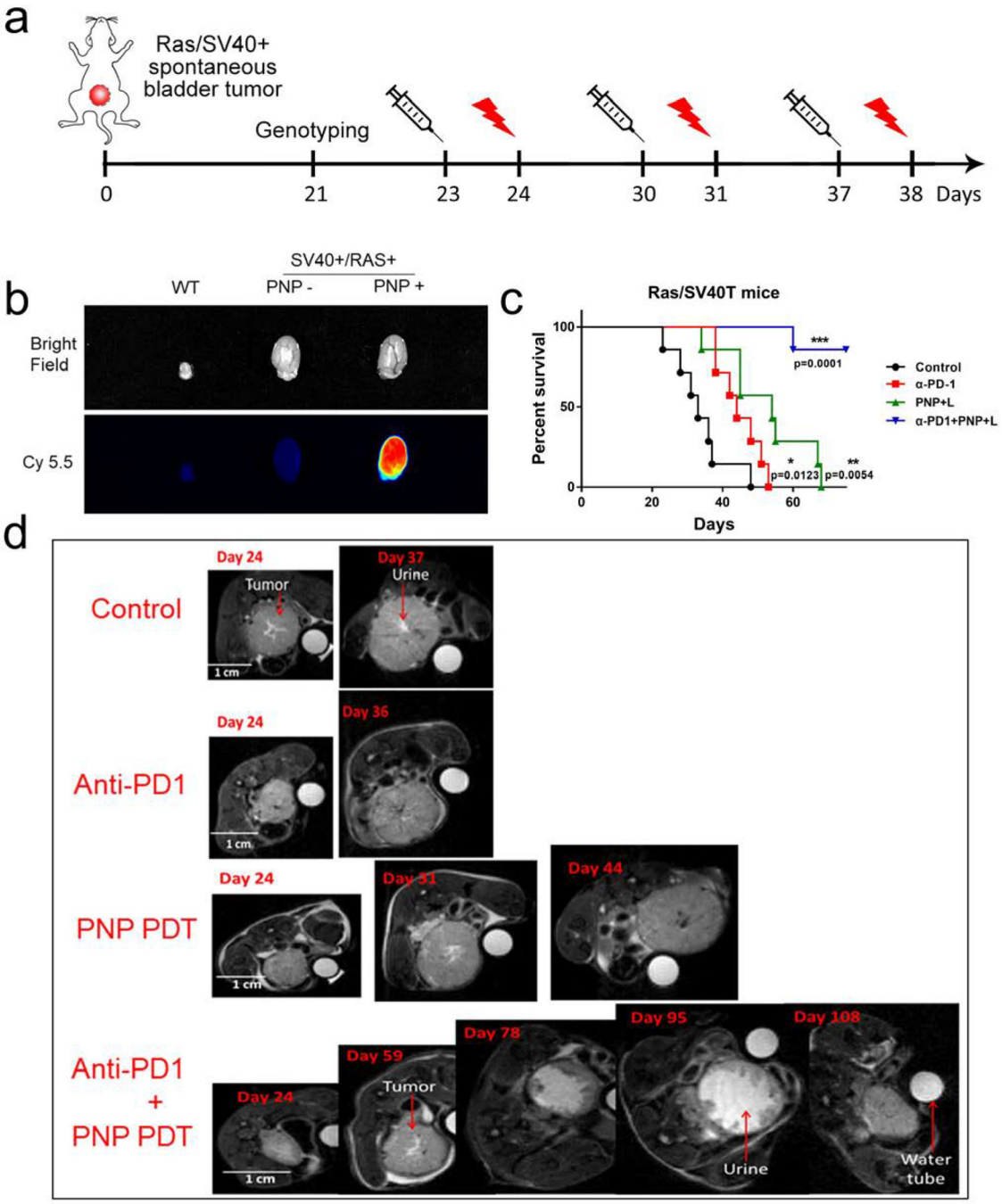

Figure 2: Synergistic anti-tumor activity between PDT and immunotherapy in treating localized spontaneous bladder cancer.

a) Schema showing the experimental design for a SV40T/RAS* double transgenic spontaneous bladder cancer model. SV40T/RAS* double transgenic mice develop localized spontaneous bladder cancer at 20–30 days of age. **b)** Cancer-specific delivery of PNP to the mouse bladder cancer. The bladder and spontaneous bladder cancer were collected at 24 hours after intravenous injection of PNP for near-infrared imaging. Red fluorescence indicates PNP accumulation. No significant PNP accumulation in the control mice without

bladder cancer. **c)** Survival curves of SV40T/RAS* double transgenic mice with different treatments. Compared to the median survival of 33.7 days in the control group, the median survival of the anti-P1, PNP + light and combination groups were 44.8 (p=0.0123), 52.6 (p=0.0054) and over 75 days (p=0.0001), respectively. Only 1 out of 7 mice died in the combination group at Day 75 when all mice in other groups died and the study ended. **d)** MRI image of mouse tumors after different treatments. T2 images were shown here. The white circle in each image is a water tube used as an internal control as mice and bladders changed in size over time when mice grew. The white irregular area at the central of each image is urine, especially as shown in the image taken on Day 95. In the mouse of the combination group, the effective bladder cavity area (irregular white area in the middle of the bladder representing urine) significantly increased at Day 78 and 95 and the bladder overall volume decreased while the bladder volume increased over time in the other three groups. This mouse died at Day 158.

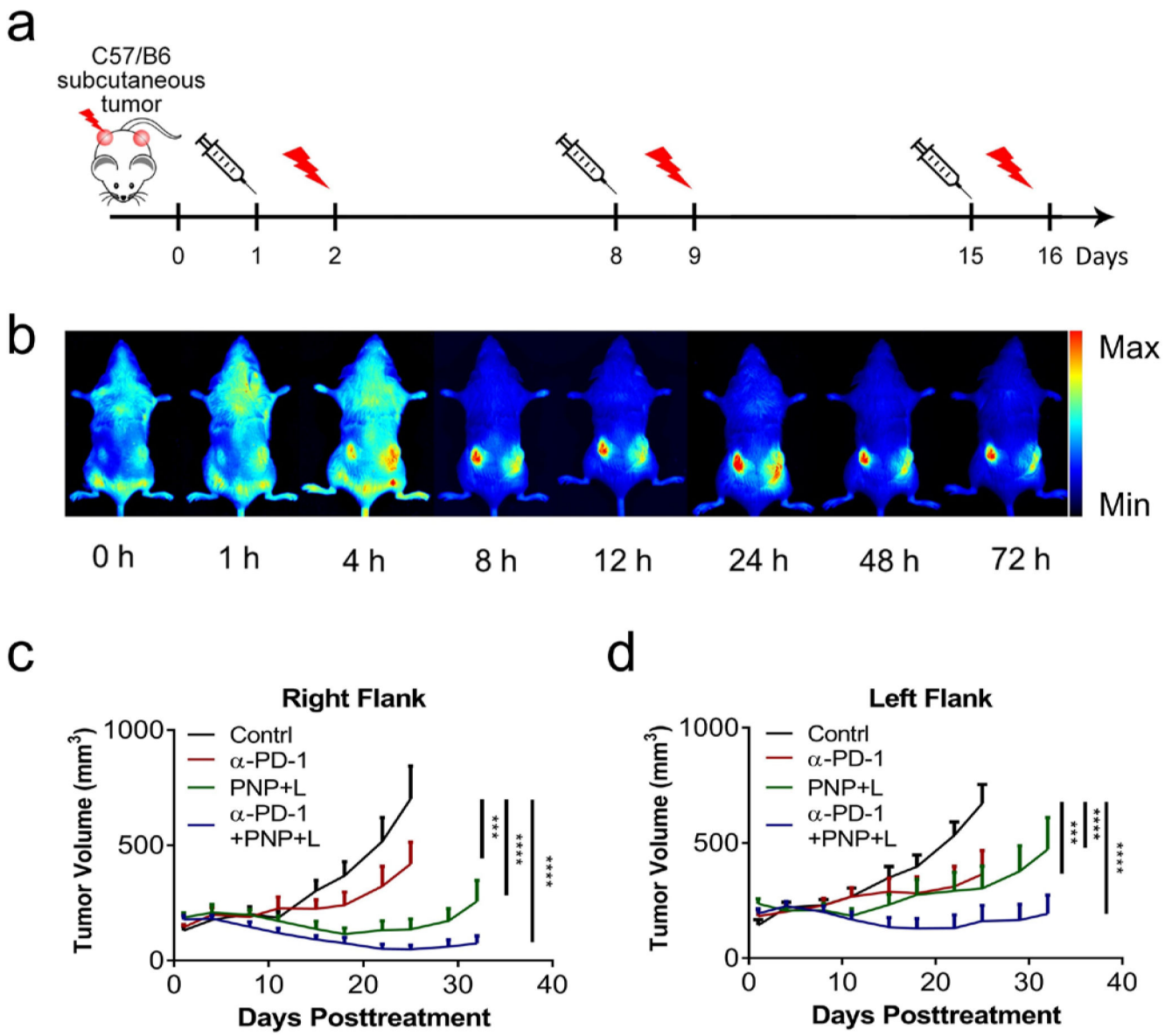

Figure 3: Synergistic local direct and abscopal anti-tumor activity of PDT and immunotherapy.

a) Experimental design for the bilateral tumor model. C57BL/6 mice bearing BBN963 subcutaneous tumors at both flanks were used in this experiment. When tumors reached the size of around 100 mm^3, tumors on the right side were treated with light for PDT and monitored for local direct anti-tumor activity. The tumors at the left flank were not treated with light and monitored for abscopal effects. **b)** In vivo fluorescence imaging to show PNP biodistribution at different time points of a C57BL/6 mouse bearing BBN963 tumors. Starting at 8 hours after administration, fluorescence from PNP accumulated at tumor sites with very little fluorescence at any other sites in the body. **c)** Tumor growth curves of the tumors at the right flank which were treated with light, showing the direct anti-tumor activities of PBS, anti-PD-1, PNP+L, or anti-PD-1+PNP+L (n=8). At day 25, compared to the control, the right-site-tumors (treated, direct anti-tumor effect) of the anti-PD-1, PDT and combination groups had a reduction of 40.25% (p=0.0003), 80.72% (p<0.0001) and

93.03% (p<0.0001), respectively. **d)** Tumor growth curves of the tumors at the left flank which were not treated with light, showing the abscopal anti-tumor activities. At Day 25, compared to the control, the tumor reduction of the left-site-tumors (measuring the abscopal effect) in the anti-PD-1, PDT and combination groups was 45.73% (p=0.0001), 54.92% (p<0.0001) and 75.96% (p<0.0001), respectively. The tumor reduction between the PDT with PNP and anti-PD-1 therapy groups was not statistically different (p=0.8402).

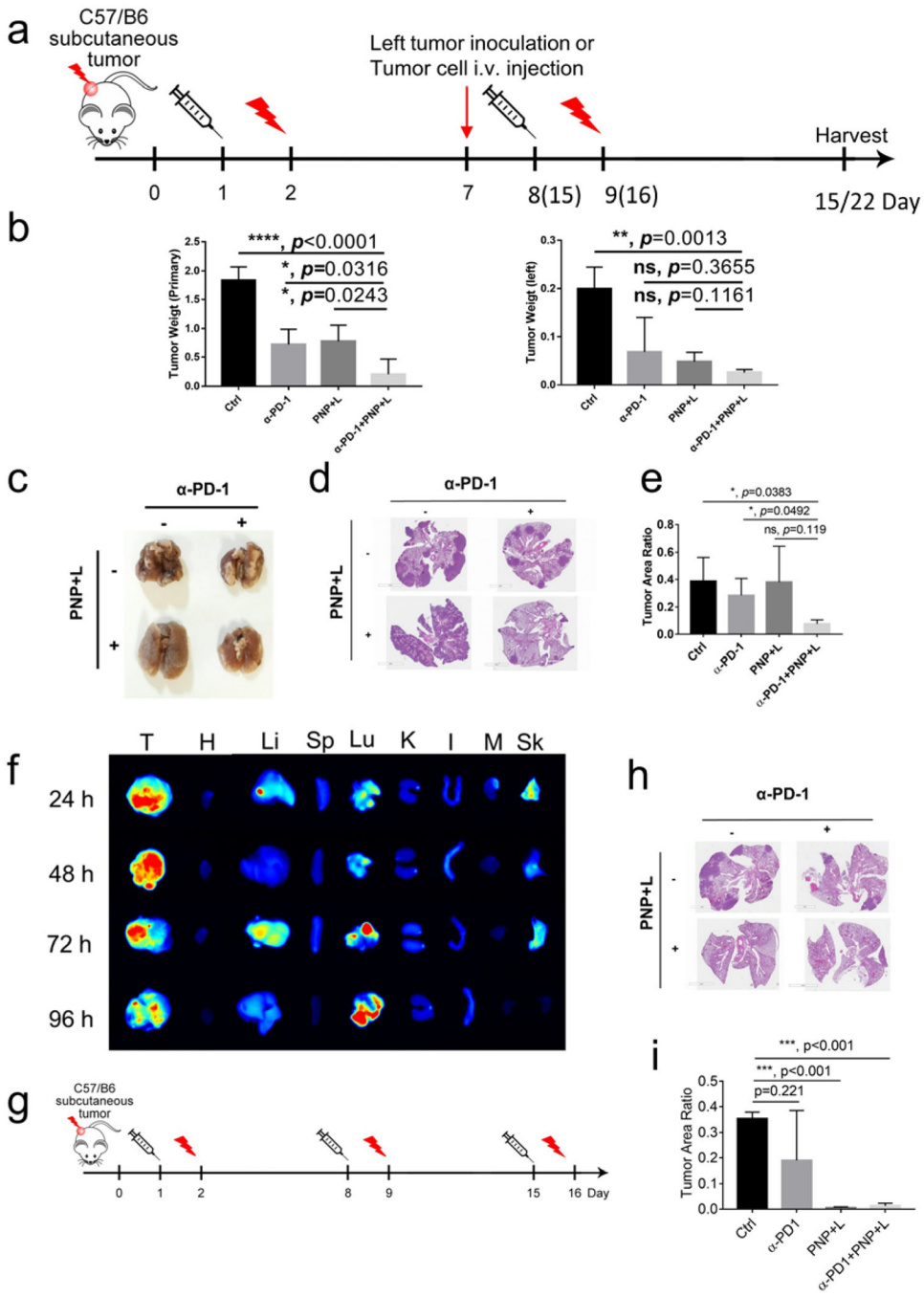

Figure 4: Synergistic PNP and immunotherapy for in vivo suppression of distant tumors and lung metastasis.

a) Experimental design to determine whether PDT and immunotherapy could prevent development of induced distant metastasis. MB49(1×10^6 cells) tumor implants were first established at the right flank of C57BL/6 mice. When tumors reached the size of 100 mm^3, mice received PBS or PNP (Day 1) followed by light treatment at the right flank 24 hours later (Day 2), and anti-PD-1 treatment was given twice a week. The same set of treatment was repeated once in the groups mimicking distant metastasis and twice

in the groups mimicking lung metastasis. MB49 cells (1×10^6 cells) were injected to the left flank on Day 7 to determine abscopal effects. To mimic lung metastasis, MB49 cells (1×10^5 cells) were injected via tail vein on Day 7. **b)** The tumors on the right side were designated as primary tumors treated with light, and those on left side were designated as distant tumor (n=4). Tumors were harvested 15 days after the first treatment. Statistical analyses were performed with tumor weights on primary site and distant site. For the right (treated) site, tumor weight was 0.21±0.13 g in the combination treatment group, compared 1.83±0.12 g in the control group ($p<0.0001$), 0.72±0.13 g in the anti-PD-1 group ($p=0.0316$), and 0.78±0.14 g in the PNP+ PDT group ($p=0.0243$), respectively (left panel). The distant tumor in the combination group was also much smaller than that in the control (0.02 ± 0.001 gram versus 0.2 ± 0.02 gram, p=0.0013) even though not much smaller than the other two groups (right panel). **c-e** Lungs were harvested 22 days after the first treatment in the groups mimicking lung metastasis. **c)** Gross appearance of tumor nodules in the lungs. **d)** Hematoxylin and eosin staining of lungs. **e)** Statistical analysis of tumor area. The tumor/lung ratio in the combination group was smaller than the control ($p=0.0383$) and anti-PD-1 ($p=0.0492$) groups, but not the PNP plus light treatment group ($p=0.119$). **f)** fluorescent signal showing PNP accumulation in tumor and lung, suggesting development of spontaneous lung metastasis. (T: tumor, H: heart, Li: Liver, Sp: Spleen, Lu: Lung, K: Kidney, I: Intestine, M: Muscle, Sk: Skin). **g)** Schema showing the design to determine whether PDT and immunotherapy could prevent development of spontaneous lung metastasis. **h)** Hematoxylin and eosin staining of lungs. **i)** Statistical analysis of tumor area. Compared to the control, the PNP plus light treatment and the combination groups significantly decreased spontaneous lung metastasis ($p<0.001$).

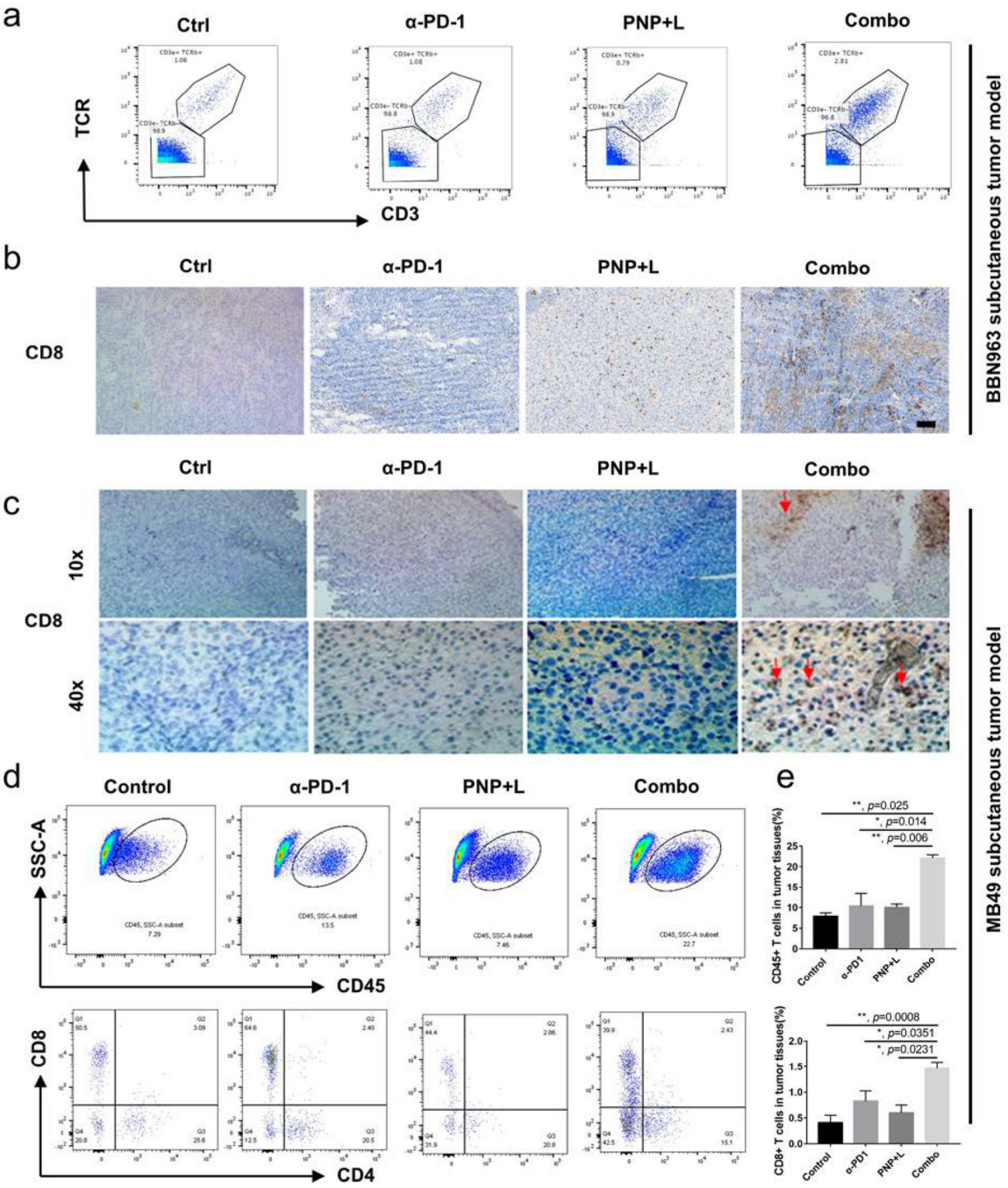

Figure 5. Synergistic effects of PNP and immunotherapy in activating systematic anti-tumor immunity.

a) CyTOF analysis of left tumor in BBN963 subcutaneous model. Of all nucleated cells in the tumors, the CD3e+TCRb+T cells in the combination treatment group was 2.81% compared to 1.06%, 1.08%, and 0.79% in the control, anti-PD-1 and PDT groups, respectively. **b)** IHC showing CD8+ T cell infiltration into left tumors (scale bar = 100 μm) of BBN963 tumors. **c)** CD8+ T cell infiltration into MB49 subcutaneous tumors. Red arrow indicates the CD8+ T cells. (Upper panel, 10X; Lower panel, 40X). In both tumor

models, significantly more T cell infiltration was observed in the combination groups. **d)** Representative flow-cytometry plots showing tumor-infiltrating leucocyte cells, including CD45+ cells and CD8+ T cells, in distant sites of the MB49 model. The numbers at the lower panel of the flow cytometry plots are percentage of CD4/CD8 cells among CD3+ cells. **e)** statistical analysis of CD45+ cells (upper panel) and CD8+ T cells of all cells in the distant tumors. The percentage of CD45+ leucocytes in the PDT with PNP plus anti-PD-1 treatment group was 22.60% in the distant tumors of the left flank that were not treated with light (abscopal effects), compared to 8.63% (p=0.025), 9.80 (p=0.014) and 9.97 (p=0.006) in the control, anti-PD-1 and PNP groups, respectively (upper panel). The percentage of CD45+CD3+CD8+ cells among all cells in the tumor in the PDT with PNP plus anti-PD-1 treatment group was 1.463% of all cells in tumor, compared to 0.408 (p=0.0008), 0.826(p=0.0351) and 0.598 (p=0.0231) in the control group, anti-PD-1 and PNP PDT groups, respectively (lower panel).